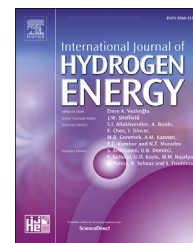




ELSEVIER

Available online at www.sciencedirect.com

ScienceDirect

journal homepage: www.elsevier.com/locate/he

Accurate measurement of pressure-composition isotherms and determination of thermodynamic and kinetic parameters of metal hydrides

Pamela Canjura Rodriguez ^{a,*}, Noris Gallandat ^{a,b,c}, Andreas Züttel ^{b,c}

^a GRZ Technologies Ltd., Energypolis, Rue de l'Industrie 17, CH-1951 Sion, Switzerland

^b Institute of Chemical Sciences and Engineering (ISIC), Basic Science Faculty (SB), École polytechnique fédérale de Lausanne (EPFL) Valais/Wallis, Energypolis, Rue de l'Industrie 17, CP 440, CH-1951 Sion, Switzerland

^c Empa Materials Science & Technology, CH-8600 Dübendorf, Switzerland

ARTICLE INFO

Article history:

Received 4 February 2019

Received in revised form

24 March 2019

Accepted 27 March 2019

Available online 24 April 2019

Keywords:

Hydrogen storage

Metal hydrides

Pressure composition isotherms

Sorption-analysis

ABSTRACT

This work presents an in-depth investigation of different techniques used to accurately determine pressure-composition isotherms (pCI) as well as thermodynamic and kinetic parameters of metal hydrides. A case study is presented for an alloy of the type LaNi₅. The results combine experimental measurements with theoretical modeling. Firstly, the numerical work presented discusses a numerical method for the evaluation of pCI raw data in order to minimize the experimental error. A simple, efficient iterative algorithm is presented to solve for the van der Waals equation of state in order to take into account the compressibility of hydrogen. Secondly, the measurements of dynamic (mass-flow) and quasi-static (Sievert's type) isotherms at different temperatures and different flow rates are presented. The dead volume of the apparatus as well as its experimental error, which is key parameter for the accurate calculation of hydrogen capacity, are also measured. Finally, important thermodynamic and kinetic parameters are deduced from the pCI curves. The kinetics of the absorption and desorption reactions are modelled and the reaction rate constants are found using both dynamic and quasi-static methods. The presented work goes beyond the calculation of the entropy and enthalpy of reaction, as the lattice gas model is also used to determine the critical temperature as well as the interaction energy between hydrogen-metal atoms and hydrogen-hydrogen atoms.

© 2019 Hydrogen Energy Publications LLC. Published by Elsevier Ltd. All rights reserved.

Introduction

Renewable energy sources such as wind and solar are sought to gradually replace conventional, fossil-based energy sources. However, there is a need for large-scale energy storage technologies in order to enable a successful transition

towards renewable energy. Hydrogen is seen as a promising energy carrier with multiple advantages such as the absence of greenhouse gases emissions and no net uses of natural resources. The biggest challenge in hydrogen technologies, however, consists in storing this gas efficiently, safely and at a high density [1–6]. Several methods exist for the storage of hydrogen, such as compressed gas, liquefaction or absorption

* Corresponding author.

E-mail address: pamela.canjura@grz-technologies.com (P. Canjura Rodriguez).

<https://doi.org/10.1016/j.ijhydene.2019.03.224>

0360-3199/© 2019 Hydrogen Energy Publications LLC. Published by Elsevier Ltd. All rights reserved.

in solid materials. Metal hydrides, complex hydrides and carbon-based materials have emerged as attractive potential solutions for the storage of hydrogen [7–11]. The advantages of sorption (adsorption or absorption) materials are several-fold: first, higher volumetric densities are usually achieved than conventional (liquid and compressed gas) storage methods. Second, sorption processes typically occur at low pressures, thus eliminating major safety risks associated with the storage under high pressure. Finally, the lack of additional processes such as compression and liquefaction increase the round-trip efficiency of the hydrogen cycle and can potentially diminish the investment costs. However, the experimental characterization of hydrogen storage materials is quite complex and requires advanced experimental setups and careful numerical evaluation [8]. For sorption process, several cases of irreproducibility have been reported in this field [12]. The characterization methods can be divided in mainly three main categories: gravimetric, volumetric and Temperature-Programmed Desorption (TPD) [12]. All these techniques allow not only the determination of thermodynamic and kinetic parameters but are also the cornerstone in the selection of an efficient material for a specific application [13].

Sorption materials are characterized by a low equilibrium pressure and a high volumetric energy density [13,14]. Metal hydrides react with hydrogen and form mainly metal-hydrogen solid compounds that have up to four times the volumetric H_2 density than liquid hydrogen [10]. The process starts with the host metal initially dissolving some hydrogen as a solid solution, also known as the α -phase. As the concentration of hydrogen increases in the metal, there are stronger local interactions between H–H leading to nucleation and growth of the hydride, also known as β -phase. There is a critical temperature T_c for the material at which the transition between α -phase and β -phase is continuous. At any temperature below this critical temperature it exists a coexistence of the two-phase region characterized by small pressure variation and a plateau in the p - V curve. The total storage capacity of the material at a constant temperature is given the length of the plateau in the isotherm [15].

This paper focuses on the characterization of the sorption capacity of metal hydrides. They are one of the most promising hydrogen sorption materials currently available at commercial scale and have been studied in multiple occasions [16–20]. This paper presents two different

volumetric methods for their characterization: the quasi-static (Sievert's type) method and the dynamic (mass-flow) method. Both methods are compared. The accurate numerical evaluation of the p - V curves is presented, alongside with a numerical scheme for the efficient solution of the van der Waals equation of state. Additionally, the kinetic parameters of absorption and desorption are extracted by varying the hydrogen flow rate. Finally, the lattice gas model is presented and the critical temperature as well as the hydrogen-hydrogen interaction energy are calculated. Knowing these different characteristics for a given material is fundamental to create a system for hydrogen storage depending on different basic conditions such as temperature, mobility, space and volume constraint. While, the concepts and experimental analysis of this publication have been applied to metal hydrides, they are general in nature and they can be implemented to any other type of sorption material.

Experimental setup

The experiments were performed on a GRZ AGAS Mano apparatus. The device allows performing both quasi-static (Sieverts Type) and dynamic (mass flow) measurements. The temperature of the sample is controlled in a precision sample holder with an accuracy of ± 1.1 °C throughout the measurement using a thermocouple. The sample temperature range of the apparatus is 25 °C–200 °C. The temperature of the sample holder is controlled with fluctuations of less than ± 0.2 °C. The data is recorded in a 2-s interval. The working principle of the GRZ AGAS Mano device is shown schematically in Fig. 1 alongside a picture of the apparatus. The flow rate of hydrogen can be controlled in the range of 0–5 Nml/min using a Brooks SLA5850 Mass flow controller. The pressure is monitored using a DCT531 sensor from BD sensor with an accuracy of 0.1% of the full range. The vacuum is monitored using a Pfeiffer TPG 361 vacuum gauge. The system can measure isotherms up to a pressure of 100 bar. The sample holder used is a GRZ high-accuracy sample holder with integrated heating and temperature measurement.

Numerical evaluation

The data obtained from the measurement device at every time step is the following: flow rate of hydrogen V , pressure

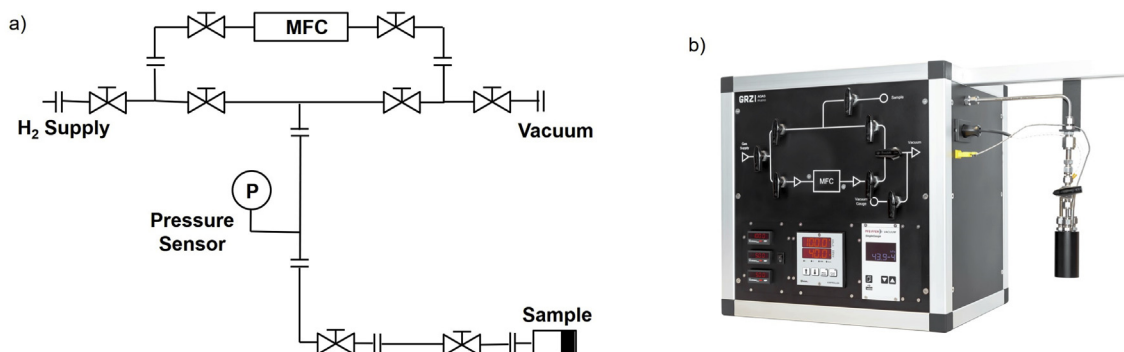


Fig. 1 – a) Schematic of the AGAS Mano b) picture of the device.

p , temperature of the sample T_{sample} and temperature of the casing T_{case} . In the first step, the flow rate of hydrogen is integrated numerically over time according to Eq. (1) in order to obtain the net amount of gas entering or leaving the system. The total volume of gas V_{tot} is then converted into a number of moles n_{tot} according Eq. (2). This number of moles includes the fraction of gas absorbed by the material as well as the gas stored in the dead volume of the system. The evaluation of the hydrogen concentration in the sample is performed following Eqs. (3)–(6). The critical step is the calculation of the amount hydrogen stored in the dead volume of the system. In many instances, the correction is made using the ideal gas law – or even neglected. This approach might lead to significant errors at higher pressures, as shown in Fig. 2. The numerical routine shown in Eqs. (4) and (5) solves the van der Waals equation of state (EOS) explicitly and converges within less than 6 iterations with an overall relative error smaller than 1×10^{-6} as shown in Table 2. The parameters for hydrogen to be used in the van der Waals equation are summarized in Table 1.

$$V_{tot}(i) = \int_0^{t(i)} \dot{V} dt = \sum_{i=0}^i \dot{V}_i \Delta t \quad (1)$$

$$n_{tot}(i) = \frac{V_{tot}(i)}{v} \quad (2)$$

$$n_{tot}(i) = n_{abs}(i) + n_{DV}(i) \quad (3)$$

$$n_{DV}^{(0)} = \frac{p(V_D - V_{Sample})}{RT} \quad (4)$$

$$n_{DV}^{(i+1)} = \frac{p(V_D - V_{Sample}) + an_i^2/(V_D - V_{Sample}) - abn_i^3/(V_D - V_{Sample})^2}{pb + RT} \quad (5)$$

$$c_{H_2} = \frac{n_{abs}M_{H_2}}{m_{Sample} + n_{abs}M_{H_2}} \cdot 100 \quad (6)$$

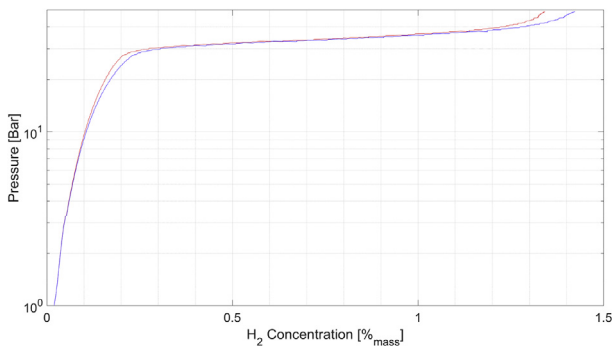


Fig. 2 – Comparison of the pCI evaluation with the ideal gas law (blue) and the van der Waals equation of state (red). (For interpretation of the references to colour in this figure legend, the reader is referred to the Web version of this article).

Table 1 – van der Waals parameters a and b for hydrogen.

Gas	a [$m^6 \cdot Pa \cdot mol^{-2}$]	b [$m^3 \cdot mol^{-1}$]
H ₂	0.02476	$2.661 \cdot 10^{-5}$

Results

Dead volume calibration

As seen in the previous section, the accurate determination of the dead volume of the system is a critical parameter for the calculation of the sorption capacity. The inaccurate consideration of the amount of gas stored in the dead volume of the system has led to several cases of irreproducibility [12]. The AGAS Mano dead volume was measured using the mass flow method at a flow rate of 5 Nml/min.

The internal dead volume was measured multiple times in order to calculate an average standard deviation for the absorption and desorption and the measurement. These were found to be 0.4% and 1.0% respectively. The results of these different measurements are shown in Fig. 3. A substantial difference in the dispersion of the results for the absorption and desorption measurements are noticed in Fig. 3. This behavior may be attributed to the different pressures at which the dead volume measurement was started. While all the absorption measurements were consistently started under vacuum conditions, the desorption measurements were performed at initial pressures that varied from 35 to 50 bar and varies throughout the measurement.

The volume was measured for absorption and desorption and the results are reported in Table 3. The difference between the absorption and desorption dead volumes is the internal volume of the mass flow controller which was found to be 0.04 cm³.

The dead volume of the system is a key parameter to determine the minimal amount of sample to be used in a measurement since the H₂ in the dead volume should not exceed the amount of H₂ stored in the sample.

pCI curves using the mass flow method

The measurements were performed on a (LaCe)(NiCoMn)₅ commercial alloy. The pCI curves were measured using the mass flow method at a flow rate of 1 Nml/min per gram of

Table 2 – Convergence of the numerical scheme for the evaluation of the number of moles stored in the dead volume.

Iteration	n [moles]	Δn [%]
p = 200 bar, T = 300 K, V = 50 cm ³		
0	0.40093	–
1	0.35107	14.203
2	0.34678	1.235
3	0.34643	0.100
4	0.34640	0.008
5	0.34640	6.80×10^{-4}
6	0.34640	5.56×10^{-5}

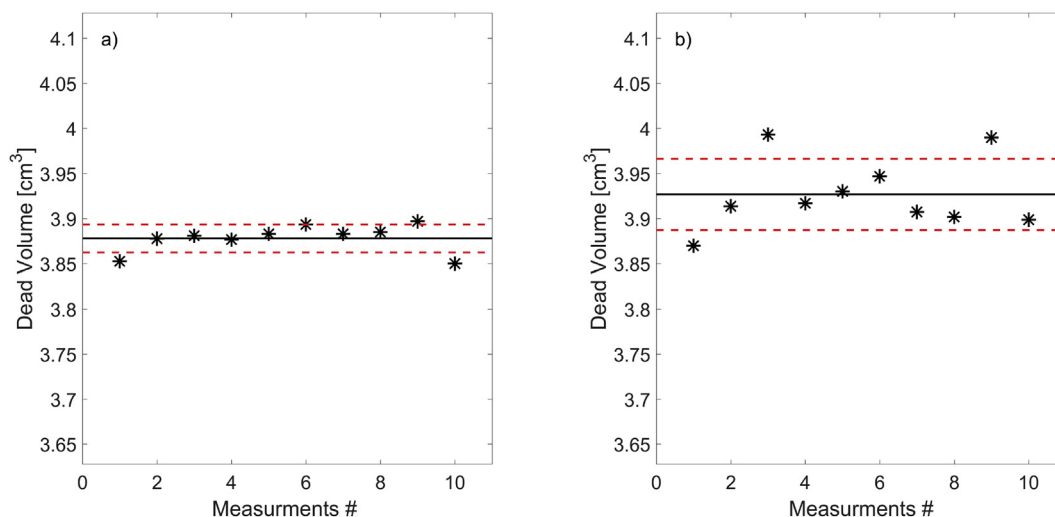


Fig. 3 – a) Measurements of the small dead volume for filling/absorption(*) and b) measurements of the small dead volume for emptying/desorption(*) were found to be 3.88 cm^3 with an average standard deviation of 0.4% and 3.92 cm^3 with an average standard deviation of 1.0%, respectively.

Table 3 – Different Dead volumes found using the mass flow method under different configurations.

Configuration	Dead Volume [cm^3]
Internal Dead Volume, Absorption	3.88 ± 0.02
Internal Dead Volume, Desorption	3.92 ± 0.04

sample with a total mass of sample of 5 g. The measurement was carried out at five temperatures ranging from $20 \text{ }^\circ\text{C}$ to $100 \text{ }^\circ\text{C}$ and the results are shown in Fig. 4. The Van't Hoff plot is extracted from the isotherms and shown in Fig. 5. The enthalpy of reaction is calculated to $-26.7 \pm 1 \text{ kJ/mol}$ (absorption) and $28.2 \pm 1 \text{ kJ/mol}$ (desorption). The entropy of reaction is calculated to $-101.0 \pm 5 \text{ J/mol-K}$ (absorption) and

$101.8 \pm 5 \text{ J/mol-K}$ (desorption). The errors were estimated from the linear regression fit obtained from the Van't Hoff plot.

An interesting feature of the mass-flow method is the possibility to perform the measurements at different flow rates, and then extrapolate the results to zero-flow rate in order to obtain the “true” equilibrium results. The isotherms at different flow rates and the corresponding extrapolation to zero-flow for the equilibrium pressure are shown in Fig. 6. From this figure, it can be observed that the “true” equilibrium pressure for absorption is higher than the “true” equilibrium pressure for desorption. This phenomenon, known as hysteresis, has been widely investigated by Flanagan et al., Qian and Northwood and Tanaka [21–24]. As the flow rate is increased, the hysteresis effect also increases as it can be noticed in Fig. 6b. This difference is due to the kinetic effects

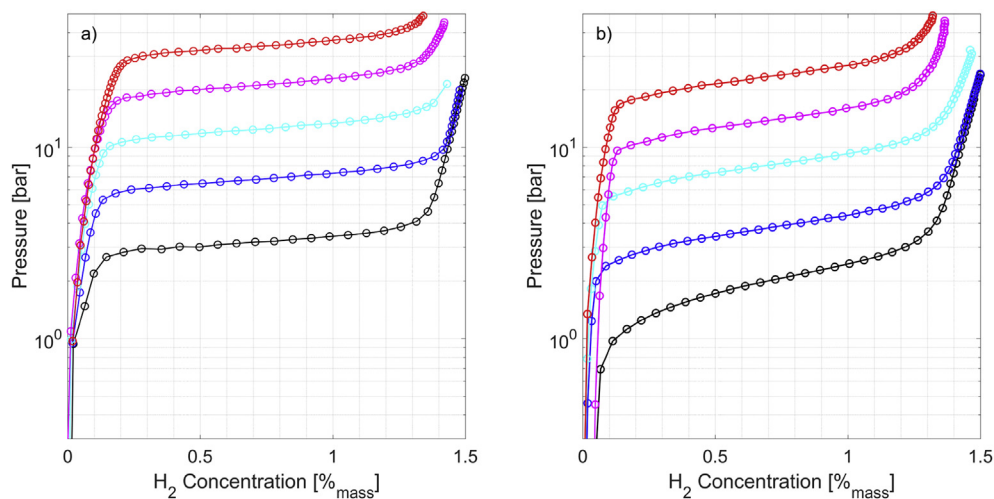


Fig. 4 – a) Absorption and b) desorption isotherms at $20 \text{ }^\circ\text{C}$ (black), $40 \text{ }^\circ\text{C}$ (blue), $60 \text{ }^\circ\text{C}$ (cyan), $80 \text{ }^\circ\text{C}$ (magenta) and $100 \text{ }^\circ\text{C}$ (red). (For interpretation of the references to colour in this figure legend, the reader is referred to the Web version of this article).

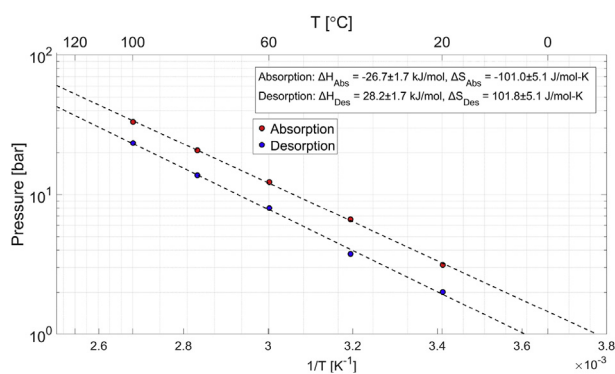


Fig. 5 – Van't Hoff plot derived from the isotherms for absorption (red) and desorption (blue). The enthalpy of reaction is calculated to -26.7 kJ/mol (Absorption) and 28.2 kJ/mol (Desorption) and the entropy of reaction is calculated to -101.0 J/mol-K (Absorption) and 101.8 J/mol-K (Desorption). (For interpretation of the references to colour in this figure legend, the reader is referred to the Web version of this article).

that increase as the flow rate used in the measurement is increased.

pCI curves using the sieverts (quasi-static) method

The Sieverts method is a sequential process where a filling or draining of two connected volumes takes place. As a first step, the reference volume is filled up until it reaches a pressure p_i . The second volume, which is where the sample is placed, is then put in contact with the first volume via the opening of a connecting valve. Once the pressure is stabilized, the connecting valve is closed and the pressure is recorded as the equilibrium pressure p_{eq} . The process is repeated until the

equilibrium pressure reaches a given value. The desorption measurement is made by an inverse procedure where the valve connected to vacuum is opened to pump out the volume of the sample. The numerical evaluation for this method is analog to the one presented in the previous section. The pCI curve obtained using the Sieverts method is shown in Fig. 7 alongside with the pCI curve obtained using the mass flow method. As it can be observed there is a difference between the plateau pressure found in the Sieverts and mass flow method. The low plateau pressure measured in the Sieverts mode, which is closer to the true equilibrium value, is due to the reduction of kinetic effects.

An overview of the different advantages and disadvantages between the two different methods are shown Table 4.

Determination of the kinetic parameters

The first study on the kinetics of alloys of LaNi_5 was made by Boser in which a constant volume apparatus was used [25]. Since then, the kinetics of the hydrogenation reaction of different variations LaNi_5 alloys under different conditions. On one hand, purely numerical and simulations have been made [17,26,27]. On the other hand, experimental methods at variable pressure conditions and constant pressure made by Suda et al. [28] and Miyamoto et al. [29]. The latter work reported values for the reaction constant at 40°C of 0.01 s^{-1} and activation energies of 32.7 kJ/mol H_2 . However, no study has modelled and deduced the kinetics of the reaction from the pCI curves measurements at different flow rates. This work will address this gap. The pCI curves found using the mass flow method shown in the previous section were used to determine the kinetic parameters of the hydrogen sorption reactions. The following assumptions were taken in consideration. Firstly, since the flow consists of pure hydrogen, there are no diffusion limitations in the gas phase of the reaction. Secondly, the rate of absorption and desorption may be

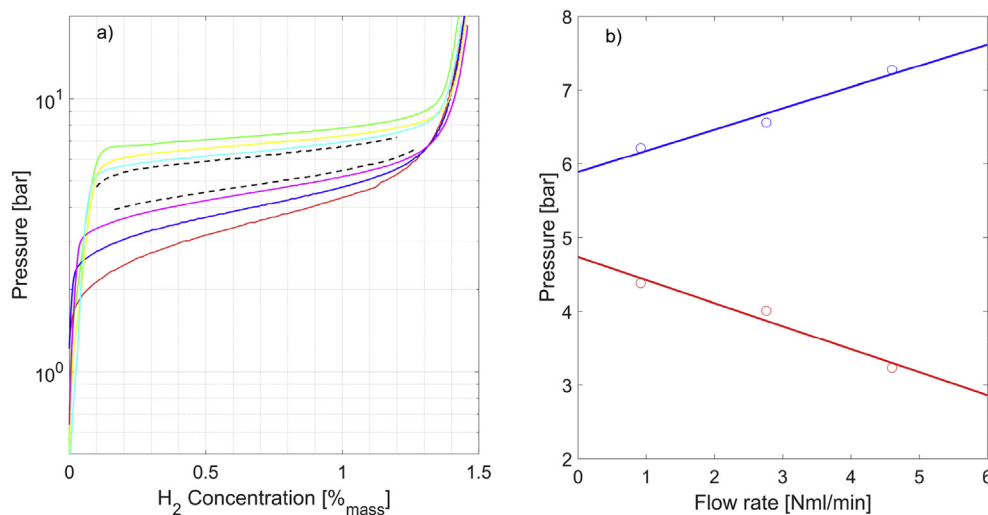


Fig. 6 – a) Isotherms at different flow rate for absorption at 5 Nml/min (green), 3Nml/min (yellow), 1Nml/min (cyan), zero flow extrapolation (black) and for desorption at 5Nml/min (red), 3Nml/min (blue) and zero flow extrapolation (black). b) Extrapolation to zero-flow for the calculation of the “true” equilibrium pressure for absorption (blue) and desorption (red). (For interpretation of the references to colour in this figure legend, the reader is referred to the Web version of this article).

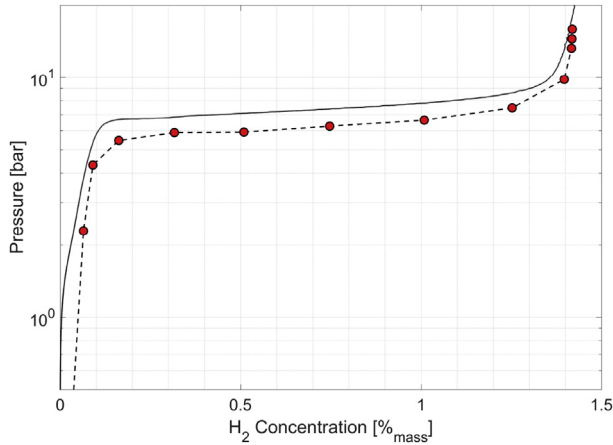


Fig. 7 – The dynamic (mass-flow, black) measurement and the quasi-static (Sievert's type, red) measurement are compared. Because of kinetic effects, the equilibrium pressure measured in the quasi-static mode is lower than the pressure measured in the dynamic mode. (For interpretation of the references to colour in this figure legend, the reader is referred to the Web version of this article).

described at any hydrogen concentration within the two-phase region using the formula (7). This formula is a first approximation in which the rate of the reaction is determined by a linear mass transfer from the metal surface to the α -phase/ β -phase interface. A graphical representation of this phenomena is shown in Fig. 8.

$$r_{abs/des,H_2} = k_{abs/des} \left| (p_{eq} - p) \right| \quad (7)$$

The rate of absorption can be considered proportional to the rate of hydrogen supply since the two-phase region is characterized by only a small variation of the pressure in the system [16]. In fact, the portion of the flow of hydrogen supply that does not react with the metal hydride is relatively constant and may be defined as a factor f . For this system, this constant f represents 8% of the initial flow rate. Therefore, the rate of absorption in the system may be written as shown in Eq. (8) and Eq. (9).

$$r_{abs/des,H_2} = \frac{\partial n_{abs/des}}{\partial t} = \frac{(1-f) p_n}{RT_n} \dot{V} \quad (8)$$

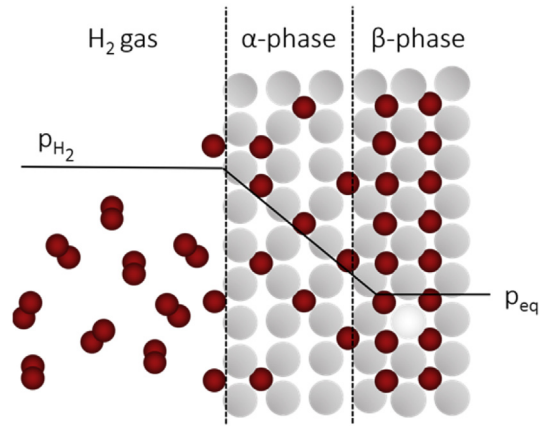


Fig. 8 – Graphical representation of the absorption phenomena for a metal in the two-phase region. The driving force for the absorption is the gradient between the applied hydrogen pressure and the equilibrium pressure.

$$\dot{V} = \frac{k_{abs/des} RT_n}{(1-f) p_n} (p_{eq} - p) \quad (9)$$

The value of k_{abs} may be obtained at each point of the plateau using the slope of a linear extrapolation similar to the one made for the plateau pressures shown in Fig. 6. The different rates of absorption and desorption were calculated along the two-phase region and the results are shown in Fig. 9 and Fig. 10. The absorption rate constant was found to be $2.6 \times 10^{-11} \text{ mol s}^{-1} \cdot \text{Pa}^{-1}$ with average standard deviation of 3%. Similarly but under a slightly reduced range concentration range of 0.1–1 %wt, the average desorption rate constant found was $2.5 \times 10^{-11} \text{ mol s}^{-1} \cdot \text{Pa}^{-1}$ with an average standard deviation of 11.0%. This range was selected to better match the desorption plateau pressures observed in Fig. 6. Two quite distinct behaviors were observed for the absorption and desorption reactions rates. On one hand, the absorption rate constant remained relatively constant for all hydrogen concentration with an average standard deviation of 2.5%. On the other hand, the desorption rate constant decreased as the concentration of hydrogen decreases in the two-phase region. Therefore, the first approximation for the diffusion of hydrogen shown in Eq. (9) does not properly describe the process of desorption. This could be due to the constraint that the system has in

Table 4 – Comparison of the two volumetric characterization methods studied.

Method	Advantages	Disadvantages
Sieverts (quasi-static)	<ul style="list-style-type: none"> Reduces the kinetic effects and therefore a closer pressure of equilibrium is found in a single measurement 	<ul style="list-style-type: none"> User interaction required at each step, increases the possibility to human error and demands active monitoring Sequential measurement method; no continuous curve Longer time for measurement (up to 2x as compared to dynamic)
Mass Flow (dynamic)	<ul style="list-style-type: none"> The measurement only requires an initial set-up and no additional user manipulation nor active monitoring The time for measurements can be as low as half of that using the Sieverts method Continuous data acquisition results in a smooth curve 	<ul style="list-style-type: none"> Measurements at high flows determines plateau pressures with a relative error of up to 20% due to kinetic effects.

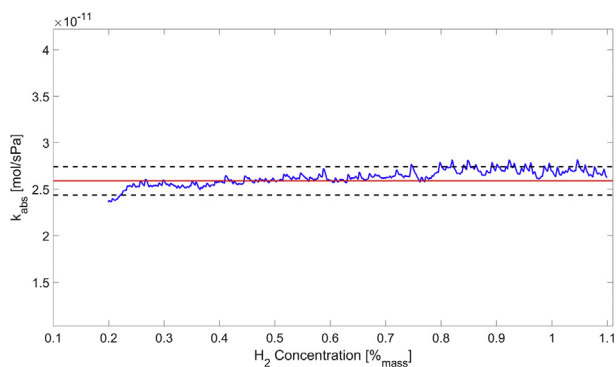


Fig. 9 – Rate constants for absorption calculated using the mass flow method over the plateau-region for the alloy $(\text{LaCe})(\text{NiCoMn})_5$ at $40\text{ }^\circ\text{C}$ (blue). The average absorption rate constant was found to be $2.6 \times 10^{-11} \text{ mol}^{-1}\text{Pa}^{-1}$ (red) and an average standard deviation of 5.1%. (For interpretation of the references to colour in this figure legend, the reader is referred to the Web version of this article).

the desorption mode, in which there is a maximal pressure gradient set by the minimal physical attainable pressure which is 0 and consequently the pressure gradient cannot linearly progress with the reaction rate but rather has a decaying behavior.

The kinetics of the reaction may also be studied using the data obtained for the Sieverts method. The rate of absorption and desorption may be described using Eq. (7). The behavior observed in pressure at each step of the Sieverts method may be modeled as an exponential decay from the initial pressure in the reference volume V_{ref} to the equilibrium pressure in the overall volume V_{final} as shown in Eq. (10). Similarly, the change of pressure drop at each time can be described using Eq. (11). This approximation was made for 5 different points in the

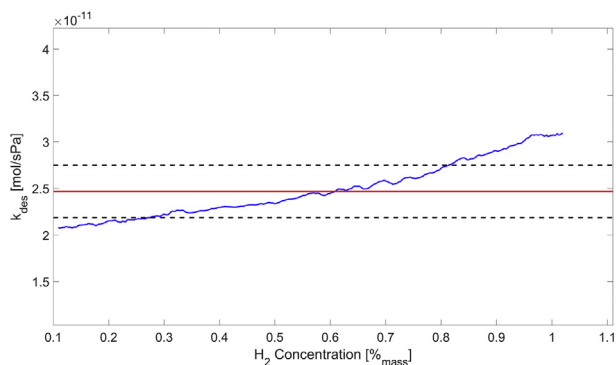


Fig. 10 – Rate constant for desorption calculated using the mass flow method over the plateau region for the alloy $(\text{LaCe})(\text{NiCoMn})_5$ at $40\text{ }^\circ\text{C}$ (blue). The average desorption rate constant found was $2.5 \times 10^{-11} \text{ mol s}^{-1} \text{ Pa}^{-1}$ (red). The desorption rate constant exhibits a decreasing behavior with an average standard deviation of 11.4%. (For interpretation of the references to colour in this figure legend, the reader is referred to the Web version of this article).

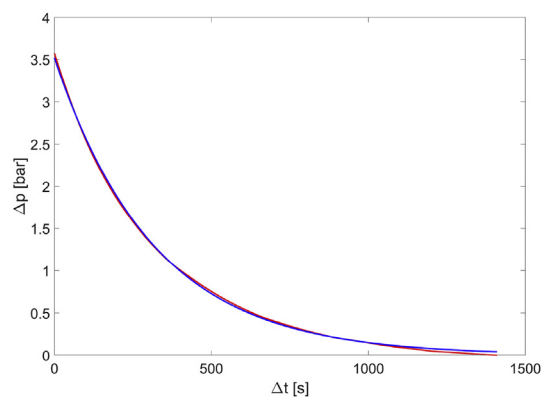


Fig. 11 – The pressure evolution at a single step of the Sieverts method (red). The behavior may be fitted as an exponential decay from the initial pressure in the reference volume V_{ref} to the equilibrium pressure in the overall volume V_{final} (blue). (For interpretation of the references to colour in this figure legend, the reader is referred to the Web version of this article).

plateau area of the pCl curve and one of the fittings is shown Fig. 11.

$$\Delta p = ae^{-bt} \quad (10)$$

$$\frac{\partial \Delta p}{\partial t} = -abe^{-bt} \quad (11)$$

This change in pressure may be linked to the rate of the reaction since the number of moles absorbed is the difference between the initial moles at the referral volume and the final moles in the total volume. Hence, the change in the number of moles is proportional to the change in the pressure drop as shown in Eq. (12).

$$\frac{\partial n_{\text{abs}}}{\partial t} = \frac{\partial n_{V_{\text{ref}}} - \partial n_{V_{\text{final}}}}{\partial t} = \frac{\partial \Delta p}{\partial t} \frac{(V_{\text{ref}} - V_{\text{final}})}{RT} \quad (12)$$

Thus, by substituting Eq. (11) in Eq. (12) and comparing it to Eq. (7), k_{abs} can be defined as shown in Eq. (13). The value of k_{abs} may be calculated at different points within the two phase region and the results are shown in Fig. 12

$$k_{\text{abs}} = b \frac{(V_{\text{ref}} - V_{\text{final}})}{RT} \quad (13)$$

These values are consistent with the ones found for the rate constant using the mass flow method since the average of the rate constant found in the Sieverts method only varies 0.6% from the average found in the mass flow method.

Lattice gas model and H–H interaction energy

The lattice gas model considers the alloy as a lattice of the metal atoms and the hydrogen to be placed in the interstitial sites as a mobile free gas H atom. The simplest mean-field description of a lattice gas considers only the interaction of the nearest neighboring atom. The zero energy is taken as the zero energy of a single H-atom outside the metal and therefore the energy of dissolved hydrogen atoms may be written as shown in equation (14).

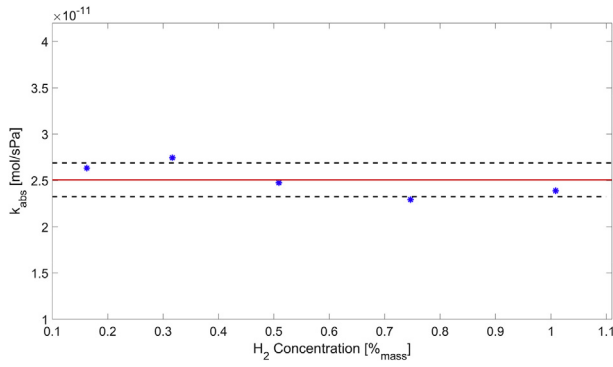


Fig. 12 – Rate constants for absorption calculated using the Sieverts method at five different points in the plateau for the alloy (LaCe)(NiCoMn)₅ at 40 °C (blue). The absorption rate constant was found to be $2.6 \times 10^{-11} \text{ mol s}^{-1} \text{ Pa}^{-1}$ (red) with an average standard deviation of 7.2%. (For interpretation of the references to colour in this figure legend, the reader is referred to the Web version of this article).

$$E = N_H \epsilon_0 + N_{HH} \epsilon \quad (14)$$

Where, N_H is the total number of sites occupied by H-atoms, N_{HH} is the total number of nearest neighbor H-pairs, and ϵ is the H–H pair interaction and the energy level of the hydrogen atom outside of the metal. The treatment of the free energy assuming that the Bragg and William condition that there is no short range order around hydrogen atoms and that at thermal equilibrium at the two phase are equal gives the Eq. (15) that describes the solubility isotherm in the one phase region.

$$\ln \left(\frac{p}{p_0} \left(\frac{1 - c_H}{c_H} \right)^2 \right) = \frac{2\epsilon_0 - \epsilon_b + 2\epsilon n c_H}{kT} \quad (15)$$

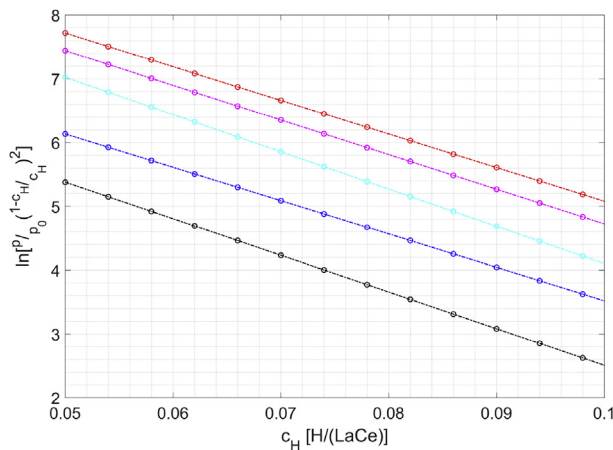


Fig. 13 – Solubility isotherms for the α -phase at 20 °C (black), 40 °C (blue), 60 °C (cyan), 80 °C (magenta) and 100 °C (red). (For interpretation of the references to colour in this figure legend, the reader is referred to the Web version of this article).

Where c_H is the ratio between occupied by H-atom sites and the total number of sites, ϵ_b the dissociation energy of a hydrogen molecule and n is the number of nearest neighbors' interstitial sites. The critical temperature is shown in (16) and it is obtained from the maximum of the temperature as a function of c_H with the critical concentration $c_H = c_c = 1/2$.

$$T_c = \frac{\epsilon n}{4k} \quad (16)$$

Using Eq. (15) and the known value of $\epsilon_b = -4.46 \text{ eV}$ for the dissociation energy of a hydrogen molecule, the energy level of the hydrogen atom outside of the metal and the H–H interaction energy are calculated to $\epsilon_0 = 2.12 \text{ eV}$ and $\epsilon n = -0.28 \text{ eV}$, respectively as shown in Fig. 13. Eq. (16) can be used to determine the critical temperature. The critical temperature T_c is calculated to 815 K. This critical temperature may be also calculated using the data found in Fig. 5 and Eq. (17). The value found was 1800 K. This value does not match the value found using the Eq. (17). This is due to two main factors. Firstly, the validity of equation only holds if the Van't Hoff plots are linear and if the temperature of the measurement are close to the critical temperature. Secondly, the experimental error expected for the T_c using equation is 333.3 K which corresponds

$$T_c = \frac{\Delta H_{abs} - \Delta H_{des}}{\Delta S_{abs} - \Delta S_{des}} \quad (17)$$

Conclusion

A thorough study of the thermodynamic and kinetic properties of the alloy (LaCe)(NiCoMn)₅ has been made via two different volumetric characterization techniques: the mass flow (dynamic) and Sieverts (equilibrium) methods. Both methods allow the accurate determination of the sorption capacity of the metal hydride with a good reproducibility. However, there are main differences in the pCl curves obtained that allows the comparison of the different methods. On one hand, the mass flow method generates a measurement in 2 s intervals that allows smoother and continuous results. This method allows the extrapolation to zero-flow in order to find the true equilibrium pressure. On the other hand, the Sieverts method reduces the kinetics effect and therefore a closer pressure of equilibrium is found in a single measurement. However, the sequential technique requires a larger number of steps and increases the risk of experimental uncertainty and the time of the measurement. Additionally, a wide range of thermodynamic and kinetic properties of the alloy were determined using the pCl results. Regarding the thermodynamic characteristics, the enthalpy and entropy for the absorption and desorption reactions were found to be $-26.7 \pm 1.7 \text{ kJ/mol}$ and $28.2 \pm 1.7 \text{ kJ/mol}$ and $-101.0 \pm 5.1 \text{ J/mol-K}$ and $101.8 \pm 5.1 \text{ J/mol-K}$, respectively. The kinetics of the absorption and desorption reaction were also studied. The rate of absorption and desorption were modelled using the diffusion of the gas through the solid. The absorption reaction matched this model fairly accurately given that the reaction rate constant was found to be $2.6 \times 10^{-11} \text{ mol}^{-1} \text{ Pa}^{-1}$ with an average standard variation of 6%. The reaction kinetics was

also calculated using the data obtained using the Sieverts method and the results were consistent with the results found using the mass flow method with a difference in average of 0.6%. Furthermore, The lattice gas model was used to determine, the critical temperature that was found to be 815 K, the energy level of the hydrogen atom outside of the metal and the H–H interaction energy that were found to be $\epsilon_0 = 2.12$ eV and $\epsilon_n = -0.28$ eV, respectively. The insight gained will be further implemented in the development and improvement of the AGAS Mano device.

Acknowledgements

Special thanks to Professor Ronald Griessen for his valuable and constructive support and suggestions on the development of this research work.

REFERENCES

- [1] Rusman NAA, Dahari M. A review on the current progress of metal hydrides material for solid-state hydrogen storage applications. *Int J Hydrogen Energy* Jul. 2016;41(28):12108–26.
- [2] Züttel A, Wenger P, Rentsch S, Sudan P, Mauron P, Emmenegger C. LiBH₄ a new hydrogen storage material. *J Power Sources* May 2003;118(1):1–7.
- [3] Schlapbach L, Züttel A. Hydrogen-storage materials for mobile applications. *Nature* Nov. 2001;414(6861):353–8.
- [4] Sakintuna B, Lamari-Darkrim F, Hirscher M. Metal hydride materials for solid hydrogen storage: a review. *Int J Hydrogen Energy* Jun. 2007;32(9):1121–40.
- [5] Peruzzini M, Poli R, editors. *Recent advances in hydride chemistry*. 1st ed. Amsterdam ; New York: Elsevier Science Ltd; 2001.
- [6] Nyamsi SN, Lototsky M, Tolj I. Selection of metal hydrides-based thermal energy storage: energy storage efficiency and density targets. *Int J Hydrogen Energy* Dec. 2018;43(50):22568–83.
- [7] Wei TY, Lim KL, Tseng YS, Chan SLI. A review on the characterization of hydrogen in hydrogen storage materials. *Renew Sustain Energy Rev* Nov. 2017;79:1122–33.
- [8] Broom DP. *Hydrogen storage materials: the characterization of their storage properties*. London ; New York: Springer; 2011.
- [9] Reilly JJ, Sandrock GD. Hydrogen storage in metal hydrides. *Sci Am* 1980;242(2):118–31.
- [10] Chandra D, Reilly JJ, Chellappa R. Metal hydrides for vehicular applications: the state of the art. *J Occup Med* Feb. 2006;58(2):26–32.
- [11] He T, Pachfule P, Wu H, Xu Q, Chen P. Hydrogen carriers. *Nat Rev Mater* Dec. 2016;1(12):16059.
- [12] Broom DP, Hirscher M. Irreproducibility in hydrogen storage material research. *Energy Environ Sci* Nov. 2016;9(11):3368–80.
- [13] Züttel A. Hydrogen storage methods. *Naturwissenschaften* Apr. 2004;91(4):157–72.
- [14] Eberle U, Felderhoff M, Schüth F. Chemical and physical solutions for hydrogen storage. *Angew Chem Int Ed* 2009;48(36):6608–30.
- [15] Chandra D. In: Walker G, editor. “12 - intermetallics for hydrogen storage,” in *solid-state hydrogen storage*. Woodhead Publishing; 2008. p. 315–56.
- [16] Biemann M, Kato S, Mauron P, Borgschulte A, Züttel A. Characterization of hydrogen storage materials by means of pressure concentration isotherms based on the mass flow method. *Rev Sci Instrum* 2009;80(8):083901.
- [17] Falahati H, Barz DPJ. Evaluation of hydrogen sorption models for AB₅-type metal alloys by employing a gravimetric technique. *Int J Hydrogen Energy* Jul. 2013;38(21):8838–51.
- [18] Van Mal HH, Buschow KHJ, Miedema AR. Hydrogen absorption in LaNi₅ and related compounds: experimental observations and their explanation. *J Less Common Met* Mar. 1974;35(1):65–76.
- [19] Li SL, et al. “Study on hydrogen storage properties of LaNi_{3.8}Al_{1.2}-xMnx alloys. *Int J Hydrogen Energy* Nov. 2010;35(22):12391–7.
- [20] Sheppard DA, Paskevicius M, Javadian P, Davies JJ, Buckley CE. Methods for accurate high-temperature Sieverts-type hydrogen measurements of metal hydrides. *J. Alloys Compd.* May 2019;787:1225–37.
- [21] Flanagan TB, Clewley JD. Hysteresis in metal hydrides. *J Less Common Met* Jan. 1982;83(1):127–41.
- [22] Qian S, Northwood DO. Hysteresis in metal-hydrogen systems: a critical review of the experimental observations and theoretical models. *Int J Hydrogen Energy* Jan. 1988;13(1):25–35.
- [23] Flanagan TB, Park CN, Everett DH. Hysteresis in metal hydrides: an illustration of entropy production. *J Chem Educ* Nov. 1987;64(11):944.
- [24] Tanaka S. “Hysteresis of hydrogen absorption (and desorption) isotherms in the α - β two-phase region of LaNi₅. *J Less Common Met* Jan. 1983;89(1):169–72.
- [25] Boser O. Hydrogen sorption in LaNi₅. *J Less Common Met* Apr. 1976;46(1):91–9.
- [26] Talagañis BA, Meyer GO, Aguirre PA. “Modeling and simulation of absorption–desorption cyclic processes for hydrogen storage-compression using metal hydrides. *Int J Hydrogen Energy* Oct. 2011;36(21):13621–31.
- [27] Zhou Z, Zhang J, Ge J, Feng F, Dai Z. Mathematical modeling of the PCT curve of hydrogen storage alloys. *Int J Hydrogen Energy* Mar. 1994;19(3):269–73.
- [28] Suda S, Kobayashi N, Yoshida K. Reaction kinetics of metal hydrides and their mixtures. *J Less Common Met* Sep. 1980;73(1):119–26.
- [29] Miyamoto M, Yamaji K, Nakata Y. Reaction kinetics of LaNi₅. *J Less Common Met* Jan. 1983;89(1):111–6.